TURBULENT CONVECTIVE HEAT TRANSFER FROM REALISTIC ICE MORPHOLOGIES

Riccardo Gaudioso
Institute of Fluid Mechanics / Department of Aerospace Science and Technology
TU Braunschweig / Politecnico di Milano
riccardo.gaudioso@tu-braunschweig.de

Barış Gökçay
Department of Aerospace Science and Technology
Politecnico di Milano
baris.gokcay@polimi.it

Antonella Abbà
Department of Aerospace Science and Technology
Politecnico di Milano
antonella.abba@polimi.it

Mariachiara Gallia
Institute of Fluid Mechanics
TU Braunschweig
mariachiara.gallia@tu-braunschweig.de

ABSTRACT

This study investigates the effects of zonal ice roughness on turbulent flow and heat transfer using Direct Numerical Simulations (DNS) of a periodic channel. Realistic ice geometries, obtained from scans of ice shapes obtained in icing wind tunnel tests, are represented via a cost-effective Immersed Boundary Method. The numerical setup is validated against reference rough-wall DNS, showing good agreement in the logarithmic and outer regions. Results demonstrate that zonal ice roughness follows trends consistent with canonical rough surfaces across transitional and fully rough regimes against equivalent sand-grain roughness. However, a clear mismatch between velocity and thermal shifts is observed, indicating an expected breakdown of Reynolds analogy. The effective slope provides a useful correlating parameter, although thermal effects consistently lag momentum transfer. These findings support zonal DNS as a robust framework for studying localized roughness and improving predictive models for icing applications.

INTRODUCTION

Aircraft icing poses a serious safety hazard for flight operation, as it degrades the aerodynamic performance of exposed surfaces. A key challenge for reliable icing prediction codes is the presence of ice roughness, which strongly modifies both skin friction and heat transfer (Guardone *et al.*, 2025). Unlike classical engineered roughness, ice formations exhibit a big variety of irregular morphologies, also depending on environmental conditions and accretion time, making their modeling particularly complex (McClain *et al.*, 2021; Sotomayor-Zakharov *et al.*, 2024). Current heat transfer models often rely on corrected Reynolds analogy approaches (Aupoix, 2015; Radenac *et al.*, 2018), but their validity under realistic icing conditions remains uncertain.

Turbulent convection over ice roughness represents a subclass of the broader problem of flows over rough walls. While the latter have been studied extensively in the context of momentum transport, the effect of roughness on heat transfer remains comparatively less understood, despite its broad relevance in environmental, geophysical, and engineering applications (Kadivar & Garg, 2025). Roughness modifies the logarithmic mean profiles of velocity $\langle u \rangle$ and temperature $\langle \theta \rangle$ through downward shifts relative to their smooth-wall counterparts (Jiménez, 2004). These profiles are commonly scaled in wall units ($^+$) through the friction velocity $u_\tau \equiv \sqrt{\langle \tau_w \rangle / \rho}$ and the friction temperature $\Theta_\tau \equiv \langle q_w \rangle / (\rho c_p u_\tau)$, being ρ the fluid density, c_p its specific heat capacity at constant pressure, and $\langle \tau_w \rangle$ and $\langle q_w \rangle$ the surface-averaged wall shear stress and heat flux, respectively:

$$\langle u \rangle^+ = \frac{1}{\kappa} \ln \left[(y-d)^+ \right] + C^+ - \Delta U^+ \left(k^+ \right), \tag{1a}$$

$$\langle \theta \rangle^+ = \frac{1}{\kappa_\theta} \ln \left[(y-d)^+ \right] + C_\theta^+ (Pr) - \Delta \Theta^+ \left(k^+, Pr \right). \tag{1b}$$

Here, $\kappa = 0.4$ is the von Kármán constant, $\kappa_\theta \approx 0.46$ (Pirozzoli *et al.*, 2016), $C^+ \approx 5.0$ and $C_\theta^+(Pr)$ are the smooth-wall log-law intercepts, d is the zero-plane displacement height, ΔU^+ is the roughness function for momentum, and $\Delta \Theta^+$ is its thermal analogue. In the fully rough regime, ΔU^+ is known to exhibit an approximately universal logarithmic dependence on roughness height once an appropriate equivalent sand roughness scale k_s is identified (Nikuradse, 1950; Schlichting, 1937). By contrast, predictive modelling of $\Delta \Theta^+$ remains considerably less mature: existing approaches are largely phenomenological, resting on restrictive assumptions and calibrated against limited datasets (Zhong *et al.*, 2023; Kadivar & Garg, 2025).

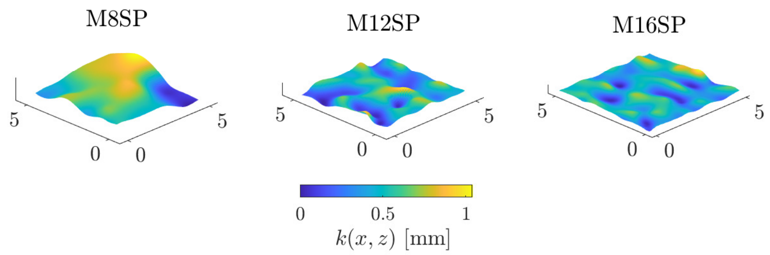

Figure 1. Rough surface samples from ice scans at $n_0 = 0.48, 0.71, 0.93$ and $t_{\mathrm{acc}} = 1.5$ min ($A_c = 0.11$). For nomenclature refer to Tab. 1. A single patch spans 5×5 mm.

Recent DNS and LES studies further indicate that momentum and heat transfer evolve differently with increasing roughness: unlike ΔU^+, which continues to grow in the fully rough regime, $\Delta\Theta^+$ tends to saturate, suggesting that a fully rough asymptotic regime for heat transfer analogous to that for momentum may not exist, especially for irregular roughness (MacDonald *et al.*, 2019; Peeters & Sandham, 2019; Zhong *et al.*, 2023; Gaudioso *et al.*, 2026). Consistent with this view, growing evidence suggests that pressure drag, which dominates rough-wall skin friction in the fully rough regime, plays only a limited role in heat transfer enhancement, which appears instead to depend primarily on viscous shear and exposed surface area (Bons, 2005; MacDonald *et al.*, 2019; Kadivar & Garg, 2025).

The simplest flow configuration to study roughness effects on turbulent flow convection is a periodic channel. While primarily used to study friction effects, this configuration has been recently extended to include heat transfer, treating temperature as a passive scalar (Forooghi *et al.*, 2018; Peeters & Sandham, 2019; MacDonald *et al.*, 2019; Zhong *et al.*, 2023). Wall geometries explored in these studies correspond to regular, synthetic, or realistic (scanned) roughness, but a very limited number of studies tackled iced surfaces. The latter can be investigated locally by reproducing friction conditions found in boundary layers of realistic airfoils, as done for example in Yang *et al.* (2023). In such work, the authors used realistic aircraft engine nacelle ice scans and introduced a zonal approach to extract ice roughness, later post-processed to cover turbulent periodic channel walls. In Hu *et al.* (2024), ice roughness effects on mean turbulence in an open channel were analyzed through DNS under pulsating pressure gradient conditions. The authors reported that the pressure gradient influenced Reynolds stresses, causing frequency-dependent phase shifts in the mean flow and leading to suppression of dispersive stress under adverse pressure gradients and enhancement under favorable ones. The main advantage of a DNS channel setup is to have a controlled, fully-turbulent simulation scenario which can be used to isolate and parametrize effects such as spatial organization of rough elements, but also flow regime effects in terms of *Re* and *Pr*. On the other hand, it must be noted that this configuration might be far from operating conditions, as it forces a fully turbulent boundary layer on top of homogeneous, periodic roughness, ignoring flow history effects and the inherently inhomogeneous geometry of realistic iced surfaces.

In this work, we systematically evaluate the effects of realistic ice morphologies using direct numerical simulations (DNS) of turbulent flow in periodic channels, enabling controlled comparisons across selected rough-wall topologies, and exploring the applicability of a simplified and flexible numerical approach to zonal ice. The study characterizes the roughness impact on mean-flow organization through the evaluation of averaged turbulent fields and log-layer shifts ΔU^+ and $\Delta\Theta^+$ over iced surfaces. By incorporating surfaces obtained from ice scans at increasing accretion times, it further assesses how the evolution of roughness features influences convective heat transfer and drag.

METHODOLOGY
Roughness generation

The generation of roughness patches is based on the unwrapping of realistic airfoil ice scans from the work of Sotomayor-Zakharov *et al.* (2024) using the Self-Organizing-Maps (SOM) technique. A set of scans produced under the icing conditions reported in Tab. 1 is here considered. Ice scans at 1.5 and 3 mins of accretion, corresponding to accumulation parameters $A_c = 0.11 - 0.21$ (a non-dimensional ice thickness measure) in mixed icing conditions are included, as roughness effects are primarily important in early stages of ice accumulation. It must be noted that 1.5 min and 3 min ice accretion represents two different icing tests and not the same continued test. Scans were obtained at different flow temperatures ($T_{\mathrm{acc}} = -8^\circ, -12^\circ, -16^\circ$ C), which are identified through the zone labels, and correspond to different freezing fractions n_0, determining the portion of impinging water mass freezing on impact, a value of 0 means no water is freezing and a value of 1 means that all the water is freezing. From these scans, local patches in the suction and pressure side region of the airfoil are extracted, resulting in an elevation map $k = k(x,z)$. The zone selection was based on the arc-length roughness height distribution, resulting in zonal morphologies such as those reported in Fig. 1 for $t_{\mathrm{acc}} = 1.5$ min. The focus is in particular on the roughness distribution peaks on the profile that lead to intrusive ice features formation, as they are associated with the strongest heat transfer enhancement. These are labeled as suction peak (SP) and pressure peak (PP) zones, ultimately associated to horns formation which severely disrupt flow quality around an airfoil (Bornhoft *et al.*, 2024).

The computational domain is a closed channel, with both walls covered by rough surfaces, as qualitatively shown in Fig. 2. A representative boundary-layer to roughness height ratio h/k was prescribed for each case based on accretion time, where h coincides with the channel half-height and k is a reference roughness height. Following previous studies on ice roughness (Yang *et al.*, 2023; Hu *et al.*, 2024), h/k was set to 18 for zones characterized by $A_c = 0.11$, while the ice obstruction was incremented with $h/k = 9$ for zones at $A_c = 0.21$. A mirroring technique was used to cover a sufficiently large domain extent for the channel simulations, namely of $4h \times 1.5h$

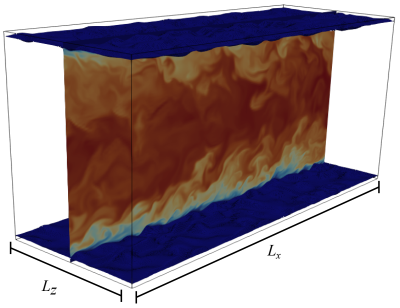

Figure 2. Turbulent periodic channel setup with immersed rough walls obtained from mirrored ice patches.

Table 1. Selection of ice roughness zones.

Zone	$n_0\,[-]$	$A_c\,[-]$	$k_{\mathrm{rms}}\cdot 10^4\,[m]$	$ES\,[-]$
M8SP	0.48	0.11 - 0.21	2.22 – 2.94	0.13 – 0.42
M12SP	0.71	0.11 - 0.21	1.07 – 3.92	0.21 – 0.56
M16SP	0.93	0.11 - 0.21	0.56 – 2.90	0.13 – 0.40
M8PP	0.48	0.11 - 0.21	2.47 – 2.62	0.28 – 0.42
M12PP	0.71	0.11 - 0.21	0.87 – 4.26	0.16 – 0.39
M16PP	0.93	0.11 - 0.21	0.74 – 3.60	0.11 – 0.39

(see Fig. 2). These dimensions were verified to be sufficient for proper turbulent structures development through a sensitivity analysis on a selected case. Additionally, the channel size is substantially larger than previous minimal channel assessments (e.g. MacDonald *et al.* (2019); Yang *et al.* (2022)), which captured an accurate flow behavior up to the log-layer for spans as low as $L_z = 0.4h$. A smoothing and edge-filtering procedure was applied to avoid abrupt surface changes and ensure periodic height profiles in span (z) and streamwise (x) direction for the numerical setup. Baseline properties and surface statistics, such as mean height k_m, maximum peak-to-valley height k_z, root-mean-square height k_{rms}, and effective slope ES, are computed as area averages from the elevation map of each zone, i.e.:

$$k_m = \frac{1}{A_t}\int_{A_t} k\,\mathrm{d}A, \tag{2a}$$

$$k_z = \max[k]\big|_{A_t} - \min[k]\big|_{A_t}, \tag{2b}$$

$$k_{\mathrm{rms}} = \sqrt{\frac{1}{A_t}\int_{A_t}(k-k_m)^2\,\mathrm{d}A}\,, \tag{2c}$$

$$\mathrm{ES} = \frac{1}{A_t}\int_{A_t}\left|\frac{\partial k}{\partial x}\right|\mathrm{d}A. \tag{2d}$$

The integrals consider a total projected wall area $A_t \equiv L_x L_z$. The computed properties are summarized in Tab. 1 for the raw patches corresponding to scan zones. These are used as reference for the mirrored and filtered computational domain, which is verified to be representative of the original roughness topology.

Numerical approach

The simulations are performed with the Xcompact3d solver (Bartholomew *et al.*, 2020), which integrates the incompressible Navier–Stokes equations with passive scalar transport:

$$\frac{\partial u_i}{\partial x_i} = 0$$
$$\frac{\partial u_i}{\partial t} + \frac{1}{2}\left(u_j\frac{\partial u_i}{\partial x_j} + \frac{\partial u_i u_j}{\partial x_i}\right) = -\frac{\partial p}{\partial x_i} + \frac{1}{Re}\frac{\partial^2 u_i}{\partial x_i \partial x_j} + f_u \tag{3}$$
$$\frac{\partial \theta}{\partial t} + u_j\frac{\partial \theta}{\partial x_j} = \frac{1}{Re\,Pr}\frac{\partial^2 \theta}{\partial x_i \partial x_j} + f_\theta$$

The geometry is discretized through a first-order Immersed Boundary Method (IBM), masking the roughness through a field function $\varepsilon(x,y,z)$ within a regular Cartesian grid stretched in the wall-normal direction. The forcing terms f_u, f_θ are computed at each time step through weighted bulk integral corrections (Cruz, 2021), which also determined iteratively the friction Reynolds number Re_τ of the simulation while maintaining no-slip, iso-scalar conditions inside the solid region ($u = 0,\ \theta = 0$). Although this approach sacrifices some accuracy with respect to second-order methods adopted in literature (Peeters & Sandham, 2019; Yang *et al.*, 2022, 2023), its simplicity significantly reduces computational cost, which is a favorable trade-off given the scope of the zonal ice study.

Table 2. Numerical-configuration summary for all rough-wall DNS cases at 1.5 and 3-minutes accretion time.

Case ID	Re_τ	h/k	$\Delta x^+, \Delta z^+$	FTT
M8SP-1.5	395, 500, 750	18	≤ 2.75	100 – 150
M12SP-1.5	395, 500, 750	18	≤ 4.22	100 – 150
M16SP-1.5	395, 500, 750	18	≤ 5.95	100 – 150
M8SP-3	500	9	3.57	≥ 125
M12SP-3	500	9	2.81	≥ 125
M16SP-3	500	9	2.31	≥ 125
M8PP-1.5	500	18	2.37	≥ 125
M12PP-1.5	500	18	3.99	≥ 125
M16PP-1.5	500	18	4.64	≥ 125
M8PP-3	500	9	4.27	≥ 125
M12PP-3	500	9	2.29	≥ 125
M16PP-3	500	9	2.61	≥ 125

Test cases

The test matrix for DNS simulations is reported in Tab. 2. The case IDs identify a specific zone according to the labels of Tab. 1, with associated ice accretion time (1.5 or 3 min). Simulation subsets are identified by a specific region, each including four temperatures resulting in different ice patches. The first subset analyses the influence of the flow regime by varying the friction Reynolds number $Re_\tau \equiv u_\tau h/\nu$. All other subsets are run at $Re_\tau \approx 500$. The influence of accretion time is investigated for each zone by comparing results at fixed Re_τ for morphologies obtained at 1.5 and 3 minutes icing. As anticipated above, the half-channel to roughness height ratio h/k is adjusted accordingly. The ratio is defined based on the maximum peak-to-valley height, i.e. $k \equiv k_z$.

Streamwise and spanwise mesh spacings in wall-units are reported (Δx^+, Δz^+). The grid required sufficient sampling for resolving turbulent scales, in line with previous DNS studies at comparable friction regimes (Busse *et al.*, 2015; Peeters & Sandham, 2019; Yang *et al.*, 2023). Moreover, to determine the adequacy of surface sampling, a number of grid points is ensured based on the minimum roughness wavelength in each direction, i.e. $\Delta x, \Delta z \leq \min(\lambda_x, \lambda_z)/12$. For all cases, the cell below roughness crests feature a first height $\Delta y_w^+ \leq 1$, able to resolve the finest turbulent scales close to the wall. At the channel center, the wall-normal mesh stretching implies a $\Delta y_{\max} \approx 5-8$ depending on the simulation case.

To extract reliable flow statistics, a double-averaging procedure in time and space is applied to compute the mean turbulent profiles such as $\langle u\rangle^+$ and $\langle\theta\rangle^+$, from which roughness-induced shifts and bulk flow quantities are also derived. Flow statistics are collected for a sufficient number of flow passages through the channel domain, measured through the flow-through-time metric $FTT \equiv L_x/U_b$, where U_b is the integral bulk velocity resulting from the constant flow rate forcing outlined in the previous section. The FTT for collection are reported, for each simulation, in Tab. 2.

RESULTS

Validation

To validate the setup, a minimal channel case is selected to test the implementation on a rough, irregular surface. Reference data from Yang *et al.* (2022) are reproduced, obtained from turbulent channel simulations on artificially generated irregular roughness. Here, case G24M2-500 is considered, which corresponds to a zero-skewness rough topology with $k_m/h = 0.016$ and effective slope $ES = 0.43$. Simulations are carried out at $Re_\tau = 500$. In the original study, a second order IBM is used to reproduce the roughness profile with a resolution of $256 \times 320 \times 48$ in a minimal span domain of dimensions $2h \times 2h \times 0.4h$. The effectiveness of this setup in capturing near-wall and log-layer behavior was demonstrated by the study. Figure 3 reports the double-averaged turbulent velocity profiles obtained from the present DNS and scaled in wall-units, where d represents the virtual origin which in this case corresponds to the moment centroid of the drag profile. A clear agreement is observed, confirming the ability of the present methodology to capture the essential roughness effects, even with a simplified surface representation. In addition, the roughness shift ΔU^+ is computed from the velocity profile (see Eq. 1a). For the present DNS, $\Delta U^+ \sim 6.29$, while Yang *et al.* (2022) report $\Delta U^+ \sim 6.30$. This result validates the usage of the current setup to study log-layer shifts with respect to equivalent sand grain roughness models.

Zonal ice analysis

In what follows, results from DNS of zonal ice are briefly summarized and discussed. Firstly, flow visualization are introduced to identify common flow features across cases, and differences between momentum and thermal transport. Then, the influence of Re_τ is analyzed for a specific subset in terms of mean turbulent fields and roughness shifts. Ultimately, the combined effect of ice morphology is targeted at a constant Re_τ, both in terms of accretion temperature – and resulting zone distribution – and accretion time, especially focusing on how the same zone evolves in influencing the mean turbulent flow.

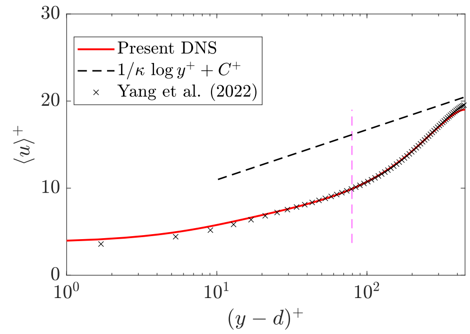

Figure 3. Mean velocity profile validation against minimal channel data from Yang *et al.* (2022). Smooth log-layers are reported (black dashed line). The vertical line indicates the location for the evaluation of roughness functions.

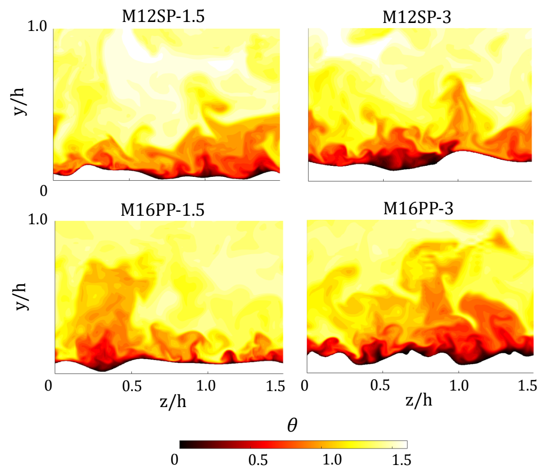

Figure 4. Inner-scaled mean temperature field (front view) for different zones (see labels).

Flow visualization To isolate the impact of ice roughness growth, the flow fields corresponding to 1.5-minute and 3-minute accretion times are analyzed comparatively on a channel yz plane mid-cut for two selected zones, shown in Fig. 4. While both stages exhibit clear roughness-induced perturbations relative to the smooth-wall reference, the dominant distinction lies in the scale, intensity, and vertical penetration of these modifications.

At 1.5-minutes, scalar transport is primarily influenced by localized crest-driven ejection events. The low-temperature region closely follows the roughness envelope, and thermal plumes remain confined to a narrow region above the crest height. In contrast, the 3-minute cases exhibit a noticeably thicker near-wall scalar layer and stronger vertical plume penetration. The coherent thermal structures extend further into the channel core, indicating that scalar transport transitions from localized roughness perturbations to canopy-scale mixing. As shown in Fig. 4, the vertical penetration of the thermal plumes is clearly enhanced at the longer accretion time.

Influence of flow regime The set of surfaces at $t_{acc} = 1.5$ min underwent a first analysis at different friction values ($Re_\tau \sim 395, 500, 750$). The 1D mean turbulent profiles, which follow the log-laws reported in Eqs. (1a) and (1b), are obtained from double-averaged DNS fields. Here, we consider the wall coordinate displaced by a virtual origin d corresponding to k_m. For clarity, we isolate the effect of Re_τ for the single M12SP-1.5 zone, as reported in Fig. 5. Analogous trends are

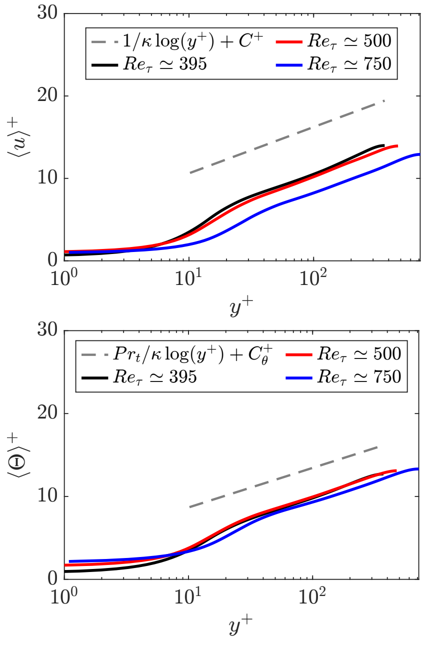

Figure 5. Mean velocity (top) and scalar (bottom) profiles for case M12SP-1.5 at varying Re_τ. Smooth log-layer trends are reported in gray.

observed for the other morphologies. The friction regime has, as expected, a primary influence on momentum: higher velocities are attained close to the rough surface, leading to the development of a thinner viscous sublayer. The effect of roughness is evident, as the logarithmic layer is shifted downward with respect to the smooth-wall reference. However, while an increase in Re_τ corresponds to a higher ΔU^+, the same trend cannot be inferred for $\Delta\Theta^+$. This indicates a mismatch in the growth of log-layer shifts across different friction regimes and suggests an increased contribution of pressure drag at higher Re_τ.

Influence of ice morphology The ice zone morphology based on accretion temperature and time heavily affects the influence on the boundary layer structure, as evidenced by flow visualizations. To analyze this aspect, we presently propose a comprehensive analysis of log-layer shifts, and their relation with selected roughness properties extracted from iced surfaces.

From DNS results, one can extract the roughness-induced shifts $\Delta U^+, \Delta\Theta^+$ in the log-layer region from the knowledge of the smooth log-law. These shifts are representative of the roughness effect on the mean flow, and can be correlated to geometrical properties through the equivalent sand grain roughness parameter, k_s. Here, the equivalent sand grain roughness is estimated by fitting Grigson´s law (Grigson, 1992) for friction in the fully rough regime, which reads

$$\Delta U^+ = 1/\kappa \log\left(1 + k_s^+ / \exp\left[-\kappa(C_N - C^+)\right]\right) \qquad (4)$$

where $C_N \simeq 8.5$ corresponds to the Nikuradse constant (Nikuradse, 1950). By knowledge of ΔU^+ from DNS, corresponding k_s^+ values can be computed for each data point by inverting Eq. 4.

The shift distributions are displayed in Fig. 6 for all zones at $Re_\tau \simeq 500$. Points are clustered based on accretion times: geometries at 3 min gather at higher k_s^+, also considering the increased h/k ratio. The thermal shift $\Delta\Theta^+$ systematically lags

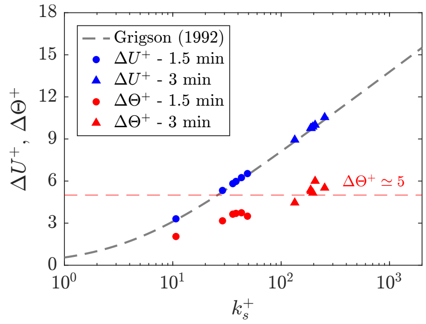

Figure 6. Momentum and thermal shifts trends versus k_s^+.

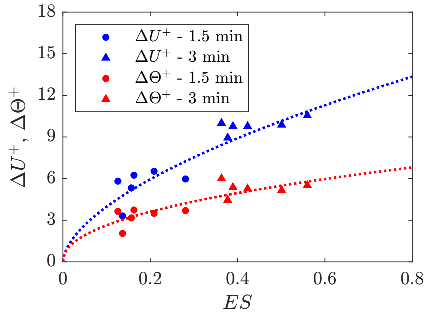

Figure 7. Momentum and thermal shifts correlation with ES.

its momentum counterpart ΔU^+. Specifically, the growth departs from the momentum one as k_s^+ increases, as a symptom of the increased pressure drag of the surface. This aspect is one of the main physical reasons for which the Reynolds analogy breaks in the presence of roughness, requiring a careful treatment of the link between global friction and convection enhancement (Peeters & Sandham, 2019; Kadivar & Garg, 2025). The relation of momentum and thermal log-layer shifts with surface geometry has been as well object of close investigation for iced surfaces, as it permits the identification of relevant surface indicators for friction and heat transfer enhancement mechanisms, respectively. By systematically evaluating the collapse of ΔU^+ and $\Delta\Theta^+$ against roughness properties, the analysis confirmed that, among others, the effective slope ES is able to collapse fairly well both ΔU^+ and $\Delta\Theta^+$. This trend can be visualized in Fig. 7. A power-law regression in log-space yielded the following scaling relations for the local roughness functions:

$$\Delta U^+ \sim ES^{0.57}, \quad \Delta\Theta^+ \sim ES^{0.46}. \qquad (5)$$

These expressions demonstrate that momentum roughness shifts increase more rapidly with slope severity than scalar roughness shifts. Indeed, eliminating ES between the two expressions gives $\Delta\Theta^+ \sim \left(\Delta U^+\right)^{0.78}$, confirming sublinear scalar response relative to momentum.

CONCLUSION

In the present investigation, the effects of zonal ice roughness on turbulent mean flow were analyzed through Direct Numerical Simulations (DNS) of a periodic channel. A cost-effective first-order Immersed Boundary Method (IBM) was used to represent elevation maps derived from realistic icing wind tunnel scans over a selected range of conditions.

The numerical setup was first validated against previous rough-wall DNS in minimal channels (Yang *et al.*, 2022), showing good agreement in both the logarithmic and outer regions.

Flow visualizations over the ice roughness were presented to provide physical insight into the mechanisms governing turbulent heat transfer. The analysis then examined the effect of flow regime (i.e., Re_τ) for a subset of cases, together with the collapse of ΔU^+ and $\Delta\Theta^+$ across transitional and fully rough regimes based on k_s^+. The results show that zonal ice roughness follows trends consistent with canonical rough surfaces, while exhibiting a mismatched growth of thermal and velocity shifts, indicating a breakdown of Reynolds analogy. The effective slope correlates well with both ΔU^+ and $\Delta\Theta^+$, although the thermal shift systematically lags the velocity shift as ES increases. Moreover, geometry-based correlations for k_s may fail for certain ice morphologies, particularly under mixed or glaze conditions, highlighting the need for careful calibration.

Overall, this study provides new insights and supports zonal ice DNS as a robust framework for investigating localized roughness effects, with potential applications in the development of improved lower-order models for icing prediction.

ACKNOWLEDGEMENTS
Funding Sources

R.G. has received funding from the European Union's Horizon Europe research and innovation program under the Marie Skłodowska-Curie grant agreement No 101072551 (TRACES). M.G. has received funding from the European Union's Horizon Europe research and innovation program under the Marie Skłodowska-Curie grant agreement No 101206621 (RESET).

The authors gratefully acknowledge the computing time made available to them on the high-performance computer "Lise" at the NHR Center NHR@ZIB. This center is jointly supported by the Federal Ministry of Education and Research and the state governments participating in the NHR (www.nhr-verein.de/unsere-partner).

REFERENCES

Aupoix, B. 2015 Improved heat transfer predictions on rough surfaces. *International Journal of Heat and Fluid Flow* **56**, 160–171.

Bartholomew, P., Deskos, G., Frantz, R. A. S., Schuch, F. N., Lamballais, E. & Laizet, S. 2020 Xcompact3d: An open-source framework for solving turbulence problems on a cartesian mesh. *SoftwareX* **12**, 100550.

Bons, J. 2005 A critical assessment of Reynolds analogy for turbine flows. *J. Heat Transfer* **127** (5), 472–485.

Bornhoft, B., Jain, S. S., Goc, K., Bose, S. T. & Moin, P. 2024 Large-eddy simulations of the NACA23012 airfoil with laser-scanned ice shapes. *Aerospace Science and Technology* **146**, 108957.

Busse, A., Lützner, M. & Sandham, N. D. 2015 Direct numerical simulation of turbulent flow over a rough surface based on a surface scan. *Computers & Fluids* **116**, 129–147.

Cruz, R. V. 2021 High-fidelity simulation of conjugate heat transfer between a turbulent flow and a duct geometry. PhD thesis, Université de Poitiers.

Forooghi, P., Weidenlener, A., Magagnato, F., Böhm, B., Kubach, H., Koch, T. & Frohnapfel, B. 2018 DNS of momentum and heat transfer over rough surfaces based on realistic combustion chamber deposit geometries. *International Journal of Heat and Fluid Flow* **69**, 83–94.

Gaudioso, R., Sotomayor-Zakharov, D. & Gallia, M. 2026 Modified scaling for turbulent heat transfer on rough surfaces. *International Journal of Heat and Fluid Flow* p. 110307.

Grigson, C. 1992 Drag losses of new ships caused by hull finish. *Journal of Ship Research* **36** (02), 182–196.

Guardone, A., Bellosta, T., Donizetti, A. & Gallia, M. 2025 Aircraft icing: Modeling and simulation. *Annual Review of Fluid Mechanics* **58**.

Hu, X., Agrawal, R., Zabaleta, F. & Yang, X. 2024 Flow over ice roughness part I. Roughness heterogeneity. *Proceedings of the Summer Program, Center for Turbulence Research, Stanford University (in preparation)* .

Jiménez, J. 2004 Turbulent flows over rough walls. *Annu. Rev. Fluid Mech.* **36** (1), 173–196.

Kadivar, M. & Garg, H. 2025 Turbulent heat transfer over roughness: a comprehensive review of theories and turbulent flow structure. *International Journal of Thermofluids* **26**, 100967.

MacDonald, M., Hutchins, N. & Chung, D. 2019 Roughness effects in turbulent forced convection. *Journal of Fluid Mechanics* **861**, 138–162.

McClain, S. T., Vargas, M. M., Tsao, J.-C. & Broeren, A. P. 2021 A model for ice accretion roughness evolution and spatial variations. In *AIAA Aviation 2021 Forum*, p. 2641.

Nikuradse, J. 1950 Laws of flow in rough pipes. *NACA Technical Memorandum* (1292).

Peeters, J. & Sandham, N. 2019 Turbulent heat transfer in channels with irregular roughness. *International journal of heat and mass transfer* **138**, 454–467.

Pirozzoli, S., Bernardini, M. & Orlandi, P. 2016 Passive scalars in turbulent channel flow at high reynolds number. *Journal of Fluid Mechanics* **788**, 614–639.

Radenac, E., Kontogiannis, A., Bayeux, C. & Villedieu, P. 2018 An extended rough-wall model for an integral boundary layer model intended for ice accretion calculations. In *2018 Atmospheric and Space Environments Conference*, p. 2858.

Schlichting, H. 1937 Experimental investigation of the problem of surface roughness. *Tech. Rep.* Tech. Rep. 823. National Advisory Committee for Aeronautics, english translation of the original 1936 publication.

Sotomayor-Zakharov, D., Radenac, E., Gallia, M., Guardone, A. & Knop, I. 2024 Statistical analysis of the surface roughness on aircraft icing. *Journal of Aircraft* **61** (1), 245–256.

Yang, J., Stroh, A., Chung, D. & Forooghi, P. 2022 Direct numerical simulation-based characterization of pseudo-random roughness in minimal channels. *Journal of Fluid Mechanics* **941**, A47.

Yang, J., Velandia, J., Bansmer, S., Stroh, A. & Forooghi, P. 2023 A comparison of hydrodynamic and thermal properties of artificially generated against realistic rough surfaces. *International Journal of Heat and Fluid Flow* **99**, 109093.

Zhong, K., Hutchins, N. & Chung, D. 2023 Heat-transfer scaling at moderate Prandtl numbers in the fully rough regime. *Journal of Fluid Mechanics* **959**, A8.